Hydrophobicity Directed Chiral Self-Assembly and Aggregation-Induced Emission

Liquid Crystals Hot Paper

How to cite: *Angew. Chem. Int. Ed.* **2022,** *61,* e202209806
International Edition: doi.org/10.1002/anie.202209806
German Edition: doi.org/10.1002/ange.202209806

Hydrophobicity Directed Chiral Self-Assembly and Aggregation-Induced Emission: Diacetylene-Cored Pseudopeptide Chiral Dopants

*Govind P. Maurya, Deepak Verma, Aloka Sinha, Luc Brunsveld, and V. Haridas**

Abstract: Here we delineate simple and tunable hydrophobically driven chiral functional assemblies of diacetylene cored pseudopeptides. These amino acid appended, rigid core dialkynes constitute promising chiral supramolecular building blocks for materials properties engineering. The chiral appended amino acid elements allow for simple tuning of solubility and interaction properties as well as governing chirality, while the central dialkyne core can impart hydrophobically driven assembly and Aggregation Induced Emission (AIE) properties. The self-assembly of these rod-like dialkynes can be regulated by tuning the solvent environment, with for example self-assembly into vesicles in acetonitrile and into helical organization with AIE in a H_2O/DMSO mixture. Of additional high interest, these supramolecular materials, themselves devoid of liquid crystal (LC) properties, can induce chirality into non-chiral LC matrices with high helical twisting power.

The design of synthetic molecules with unique self-assembling properties and ensuing chirality is a highly active area of research.[1] Nature-inspired chiral assembly integrate aggregation characteristics of both synthetic and biomolecules.[2] Also, considerable progress has been made in the design of self-assembling peptides.[3] The incorporation of molecular elements that encode for emergent functions, such as unique fluorescent properties, is a challenging endeavor.[4] Fluorescent materials have wide applications in chemical sensing, bio-imaging and in development of light emitting diodes.[5] However, aggregation-caused quenching (ACQ) of many of these materials limits their application, for example when the molecules are used in solid films.[6] Aggregation Induced Emission (AIE), opposite to ACQ, relates to an enhancement in fluorescence in the aggregated state, and such materials find numerous applications.[6,7] In order to decipher the origin of AIE, several theories have been proposed.[8] The fluorescent properties may arise due to the interaction between the transition dipoles[9] or due to the restricted intramolecular rotation (RIM).[10] Alternatively, the aggregation could cause increase in viscosity leading to blockage of molecular rotation.[11] The opportunities of peptides and related biomolecular assemblies for the development of AIE materials has not been addressed to its full potential.[10] Supramolecular chirality has been studied extensively as an additional regulatory mechanism for materials properties.[12] Combined, supramolecular chirality and self-assembling peptide-based materials offer significant opportunities for the development of self-assembling systems with emergent properties.[13] To provide urgently needed insights in self-assembling materials, AIE is an ideal concept to be utilized and incorporated into self-assembling peptide-based materials.

Functional self-assembling materials are frequently designed based on maximizing H-bonding interactions.[14] Design of self-assembling systems by controlled modulation of hydrophobic interactions is more scarce.[15] Diverse arrays of natural amino acids provide enormous design possibilities for utilizing hydrophobic interactions;[16] the diversity of amino acid side chains is the result of evolutionary tuning and is the underlying versatility of nature's design strategy.[17] Chemists are yet to optimally benefit from the rich diversity of amino acids in the design of self-assembling system.

In this work, we designed simple peptidic systems with an extended structure, reminiscent of a β-strand, with innate ability to self-assemble. We designed a rigid linear diacetylene spacer and placed amino acids derivatized with naphthalimide (NI) at its termini (Figure 1). We envisioned that such molecules with a rigid extended structure would self-assemble through intermolecular hydrogen bonding and hydrophobic interactions between the amino acid side chains. The π–π interactions between the NI units could further facilitate the self-assembly. By systematically varying the side-chains of the amino acids, the hydrophobic character of the supramolecular elements can be tuned. The rigid and extended structure of these molecules enforces and directs the intermolecular interactions, potentially coupled to a fast intermolecular polymerization. The aggregation sensitivity of the fluorescence of the NI units provides an excellent probe for investigating the self-assembly and AIE.

[*] G. P. Maurya, V. Haridas
Department of Chemistry,
Indian Institute of Technology Delhi
Hauz Khas, New Delhi- 110016 (India)
E-mail: haridasv@chemistry.iitd.ac.in

D. Verma, A. Sinha
Department of Physics,
Indian Institute of Technology Delhi
Hauz Khas, New Delhi- 110016 (India)

L. Brunsveld
Department of Biomedical Engineering, Laboratory of Chemical Biology and Institute for Complex Molecular Systems,
Eindhoven University of Technology
P.O. Box 513, 5600 MB Eindhoven (The Netherlands)

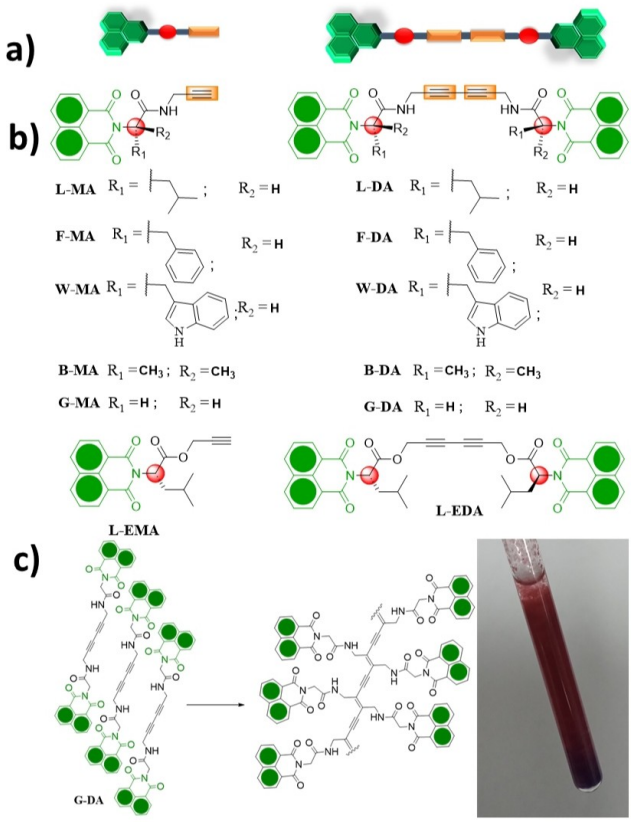

Figure 1. a) Cartoon representation of mono and diacetylene compounds. b) Chemical structures of amino acid-based monoalkynes (**L-MA**, **F-MA**, **W-MA**, **B-MA**, **and G-MA**), and diacetylenes (**L-DA**, **F-DA**, **W-DA**, **G-DA** and **B-DA)**. The chemical structures of ester derivatives **L-EMA**, and **L-EDA**, c) Polymerization of **G-DA** to polydiacetylene (PDA). NMR tube containing the PDA sample of **G-DA** illustrated by the typical red color of a PDA.

A variety of molecules with diacetylene as the core was synthesized (Scheme S1). These molecules were containing diverse amino acids with increasing side chain hydrophobicity. Out of the 20 proteinogenic amino acids Leucine (Leu), Phenylalanine (Phe), and Tryptophan (Trp) represent some of the most hydrophobic amino acids, based on a different chemical nature. The resulting materials were evaluated for their self-assembly and potential for formation of helical supramolecular arrangements, defined chirality and AIE properties.

Amino acids were appended on a rigid diacetylene spacer to form dialkynes. These are precursors for the synthesis of polydiacetylene (PDA) based peptidic polymers (Figure 1).[18] We envisaged that incorporation of NI functionalized amino acids on a PDA core may provide unusual emission properties. In addition to this, we envisioned that the NI units could also enhance the aggregation by intermolecular π–π stacking. To understand the role and the nature of the amino acid residues on the aggregation, we chose Leu (L), Phe (F), Trp (W), Gly (G) and Aib (B). The Boc-protected amino acids were reacted with propargylamine in presence of N-hydroxysuccinamide, DCC and NEt_3 in DCM, providing the monoalkynes in good yield. Deprotection followed by reaction with 1,8-Naphthalic anhydride resulted in NI-conjugated monoalkyne derivatives of the amino acids (**L-MA**, **F-MA**, **W-MA**, **B-MA** and **G-MA**). Use of propargyl alcohol instead of propargylamine yielded **L-EMA**. The dialkynes (**L-DA**, **F-DA**, **W-DA**, **B-DA**, **G-DA** and **L-EDA**) were synthesized by oxidative dimerization of the corresponding monoalkynes in the presence of Hay catalyst for 8 h. (Figure 1 and Scheme S1). The dialkyne **G-DA** already polymerized during its preparation, preventing its isolation.

For topochemical polymerization, the dialkynes must be placed at a distance of 5 Å with a tilt angle of 45°.[19] None of the diacetylenes (Leu, Phe and Trp DA-derivatives) showed polymerization, indicating that the self-assembly does not favor the distance and (or) angle criteria required for it.

Electrospray ionization mass spectra (ESI-MS) data of dialkynes showed dimer (2 M), trimer (3 M) and tetramer (4 M) indicative of aggregation (Figure S34). The rigid diacetylene core imparts a rod-like shape and ideal to self-assemble. We envisioned that these rigid molecules arrange to generate a β-sheet like arrangement, suitable for topochemical polymerization. Interestingly, none of these diacetylene (**L-DA**, **F-DA**, **W-DA**, and **L-EDA)** polymerized under normal UV irradiation, indicating the improper alignment of diacetylene units. This might arise due to bulkiness of the amino acid side chains that keep the diacetylene units at a distance unsuitable for polymerization. In order to address this issue, we synthesized Gly appended monoalkyne **G-MA** and dialkyne **G-DA**. Interestingly, **G-DA** showed polymerization suggesting that C^{α}-substitution prevents the required geometrical arrangement favorable for polymerization. The **G-DA** polymerization was so fast that, we could only isolate the polydiacetylene, which is red colored (Figure 1c). Intrigued by these findings, we set out to investigate the aggregation behavior of these compounds.

The UV/Vis absorption spectra of the dialkynes **L-DA**, **F-DA**, and **W-DA** in DMSO showed an absorption band at 333–336 nm along with a shoulder at 350–352 nm (Figure 2a and S35–S36). In 90 % H_2O/DMSO, the dialkynes showed a maximum $\Delta\lambda \approx 10$ nm bathochromic shift along with presence of long wavelength tail absorption (Figure 2a, Table S1) suggesting aggregation at this high water content. The resulting J-type aggregation is evident from the bathochromic shift.[20]

Fluorescence spectra were measured at increasing amounts of water (25–90 %, 25 °C) at $\lambda_{ex} = 345$ nm. The compounds **L-DA** and **F-DA** (Figure 2b, S35 and Table S1) showed two weak fluorescence bands at 365 and 380 nm in DMSO, attributed to the NI chromophore. A slight increase in fluorescence intensity was observed upon gradually increasing the amount of water till 60 %. As the water content increases above 60 %, a new emission band appeared at 472 nm. This intense band at 472 nm is indicative of AIE, at these more polar conditions. The dialkyne **W-DA**, in contrast, is completely non-emissive, even at high water contents. This is most likely due to a charge transfer (CT) interaction between the NI and Indole (Figure S35d).[21] The solutions of **F-DA** in H_2O/DMSO

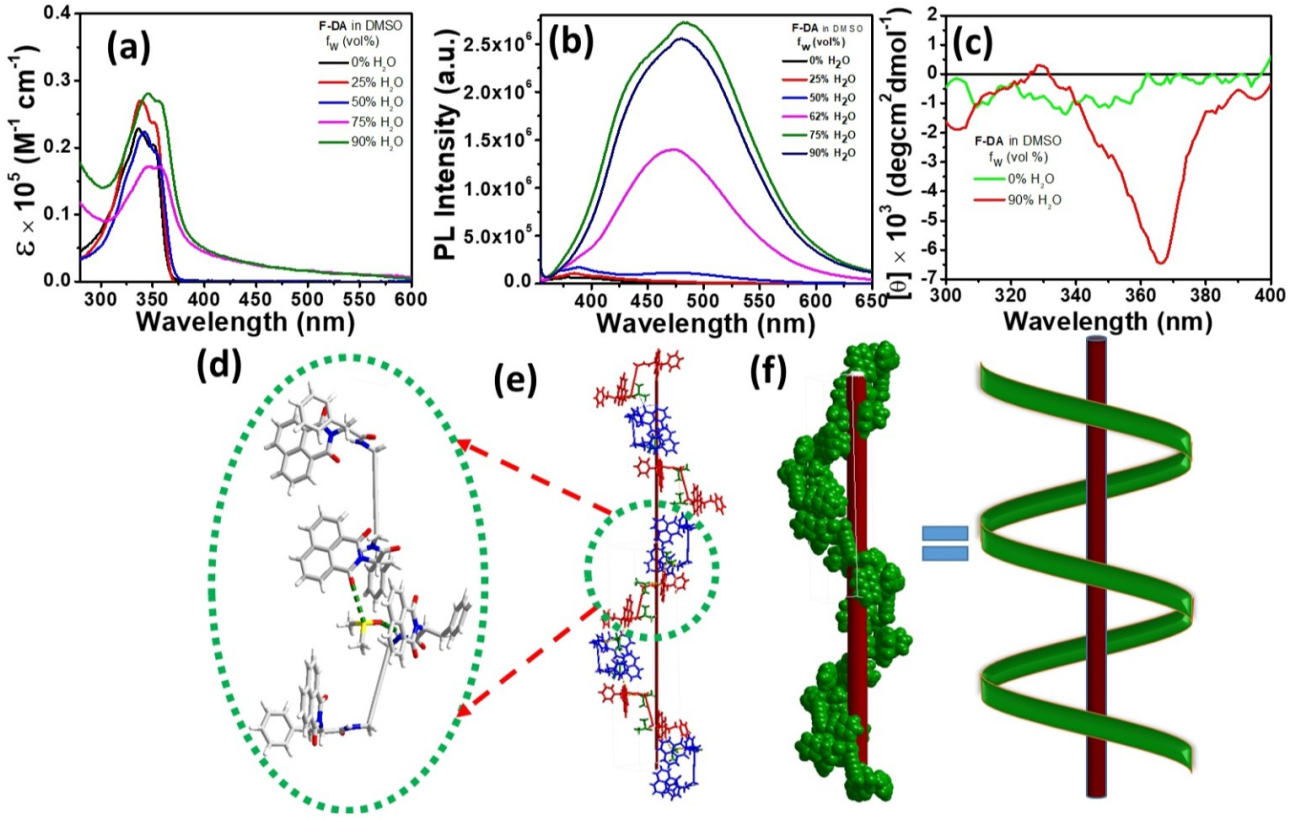

Figure 2. a) Normalized UV/Visible and b) Fluorescence spectra of **F-DA** in solutions of different H_2O/DMSO mixtures (conc. 2×10^{-5} M), c) CD spectra of **F-DA** in DMSO and 90% H_2O in DMSO (conc. 1×10^{-4} M) and d) Crystal structure of **F-DA** of two molecules showing hydrogen and chalcogen interactions with DMSO, e,f) a view of crystal packing showing left handed helical structure.

under UV light showed intense fluorescence compared to DMSO alone (Figure S37) and serve as a direct visual evidence of AIE.

The chiroptical nature of **L-DA**, **F-DA**, and **W-DA** was studied by Circular Dichroism (CD) spectroscopy (Figure 2c and S38). Addition of water showed significant CD spectral changes for the dialkyne-derivatives. The CD spectra of the dialkynes showed no evidence of chiral assembly in pure DMSO (Figure 2c and S38). The CD spectra of all dialkynes in 90 % H_2O/DMSO exhibited a negative Cotton effect at around 360–365 nm (NI unit) with the crossover point nearly corresponding to λ_{max} (UV absorption) of the NI unit, indicating a left-handed helicity of the self-assembly.[22] Since this CD signal is derived from exciton coupling, the NI moieties are stacked in a left-handed helical geometry. Exciton chirality (EC) method is used for assigning chirality to the supramolecular helical assembly. As per the EC method, the negative first and second positive cotton effect indicate a left-handed helical assembly. The CD spectra of the dialkynes in acetonitrile (ACN) were similar to that in DMSO, indicating a similar behavior in both solvents. Addition of water to ACN solution showed similar behavior as that of DMSO.

F-DA was crystallized from DMSO in the presence of a few drops of water (≈20:1). A hydrogen bond (1.94 Å) exists between amide NH of **F-DA** and oxygen of DMSO (Figure 2d). The **F-DA** molecules are hydrogen bonded through DMSO to form an extended left-handed helical (LHH) structure (Figure 2e,f). The solvent molecules interact with oxygen atoms of NI units through S···O bonds. The S···O distance and angle are 3.10 Å and 163.15° respectively (Tables S2–S3). The single-stranded helices of **F-DA** are inter-connected through C–H···π interactions between CH_2's of one helical strand and phenyl rings of another helical strand (3.54 Å) (Figure S39). Each helical structure is further connected through the NI carbonyl of one strand with CHs (NI) of another strand (2.46 Å) forming an array of helices (Figure S39). The observed LHH structure in solid state is in agreement with the helicity in solution as evident from CD data (Figure 2c). The crystal structure of **F-DA** also revealed that the closest distance between the termini of the dialkyne is 9.99 Å, which is not ideal for topochemical polymerization (Figure S40).

Electron microscopy imaging was used to probe the self-assembly process. The morphologies of the dialkynes in ACN solution (at 1 mg mL^{-1}) were investigated by scanning electron microscopy (SEM) and transmission electron microscopy (TEM) (Figure 3). SEM imaging revealed vesicles with diameter majority in the range of 400–800 nm (Figure S41). Addition of water to the ACN solutions of **L-**

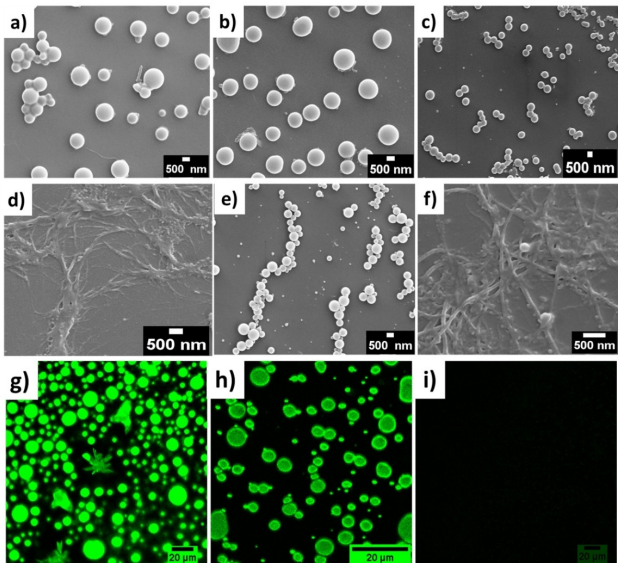

Figure 3. SEM images of a) **L-DA** b) **F-DA** c) **W-DA**. The images in a, b and c are taken from the samples made from ACN (conc. 1 mg mL^{-1}). SEM images of d) **L-DA** e) **F-DA** and f) **W-DA**. Samples for the images in d–f were made from a solution of the respective compounds in 90% H_2O and 10% ACN (conc. 1 mg mL^{-1}). Confocal images of g) **L-DA** h) **F-DA** i) **W-DA**. The samples for the confocal images are made in ACN (conc. 1 mg mL^{-1}) (λ_{ex} 405 nm).

DA and **W-DA** (9:1) resulted in the fusion of the vesicles to form fibers as evident from SEM and TEM images (Figure 3d–f and Figure S42). In the case of **F-DA**, we could image the intermediate stage of fusion (Figure 3e and S43). This fusion of vesicles is due to hydrophobic interactions, as it happens in the presence of water. Confocal microscopic imaging of **F-DA** and **L-DA** (drop-casted on a glass slide) showed green colored vesicles (Figure 3g and h) upon irradiation at 405 nm and using an observation filter in the 450–500 nm range. **W-DA** vesicles are non-fluorescent (Figure 3i), probably as a result of charge transfer interaction between the NIs and the indoles. This direct visual evidence of the non-fluorescence of **W-DA** assemblies supports the spectroscopic findings.

Encouraged by the results from the dialkynes, we investigated the aggregation of monoalkynes. The monoalkynes **L-MA** and **F-MA** are the intermediates during the synthesis of the **L-DA** and **F-DA** respectively. Compounds **L-MA** and **F-MA** (Figure 4a, Figure S44 and Table S1) are very weakly emissive in DMSO solution with emission maxima at ≈384 nm. However, when the amount of water increases, the fluorescence intensity increases with a concomitant bathochromic shift ($\Delta\lambda \approx 10$ nm) $\lambda_{em} \approx 393$ nm compared to that in DMSO alone. The increase in fluorescence intensity in H_2O/DMSO mixture is indicative of AIE. Interestingly, **W-MA** is found to be non-emissive even at higher amount of water and also this is attributed to a charge transfer (CT) interaction between the indole and NI units (Figure 4b, and e).[21]

F-MA was crystallized from DMSO. The X-ray crystal structure of **F-MA** (Figure 4c) showed that the NI and phenyl ring are in close proximity. The distances between the C–Hs of NIs and the centroid of phenyl (Phe) units are at 3.21 and 2.99 Å. The **F-MA** molecules are held together by intermolecular hydrogen bonds between amide NH and amide carbonyl (2.11 Å) and between CH of phenyl CH_2 and NI carbonyl (2.60 Å) (Figure S45 and Tables S4–S5). The CH_2 of the alkyne and centroid of NI is at a distance of 2.64 Å (Figure S45). The packing diagram shows a supramolecular left handed helical arrangement of the **F-MA** molecules (Figure 4d). Overall, the X-ray structure is consistent with observations from CD studies (Figure S46).

An X-ray quality crystal of **W-MA** was obtained from DMSO. The X-ray crystal structure revealed interactions between the amide carbonyl of one molecule and NH of the indole of Trp through an H-bond (2.04 Å) (Figure 4e, Table S6–S7). Analysis of the packing reveals that the NI unit of one molecule associates with the indole unit of another (Figure 4e and Tables S6–S8). The distance between the centroids of NI and indole is 3.63 Å, suggestive of a π–π interaction (Figure 4e). The intermolecular face to face stacking interaction between the NI and the indole is most logically responsible for the observed quenching of the fluorescence (Figure 4b). The packing diagram shows a supramolecular arrangement of NI chromophores (Figure 4f) and in agreement with the spectroscopic studies (Figure S46).

SEM imaging of the monoalkynes showed formation of vesicles (Figure S47). Addition of water to ACN solutions of **L-MA** and **W-MA** (9:1) resulted in the fusion of vesicles, whereas a rod like morphology was observed for **F-MA** (Figure S47).

The dialkynes and monoalkynes contain peptide bonds, hence hydrogen bonding could play pivotal roles in the aggregation process. To investigate this, amide linkages were replaced with ester bonds. The UV/Visible spectra of these ester derivatives (**L-EMA** and **L-EDA**) in DMSO showed two bands at 338 and 353 nm. In the 90% H_2O/DMSO mixtures, a bathochromic shift of $\Delta\lambda \approx 5$ nm was observed (Figure S48), which suggests the aggregation in the presence of water. The emission spectrum of monoalkyne **L-EMA** in DMSO showed a very weak emission band at 390 nm at λ_{ex} 345 nm, which corresponds to unassociated NI units and indicating that these are molecularly dispersed in solution. Addition of water, resulted in an enhanced intensity of the emission band at 390 nm with slight red shift.

The **L-EDA** is almost non-emissive in DMSO, while presence of water caused the appearance of a new band at 470 nm corresponding to the excimer of NI. This indicates the AIE behavior to be present in the ester derivative as well and to be promoted by water (Figure S48e). The CD spectra of **L-EDA** in DMSO did not show any band, whereas in 90% H_2O/DMSO, a negative band at around 360–365 nm (NI) with crossover point nearly corresponding to λ_{max} (UV absorption) of NI indicating left handed helical arrangement of NI units (Figure S48f). The CD results are similar to that of **L-DA**. In DMSO, the **L-EDA** is in monomeric state, whereas in 90% H_2O/DMSO it changes to chiral J-aggregates. This clearly shows that hydrophobic

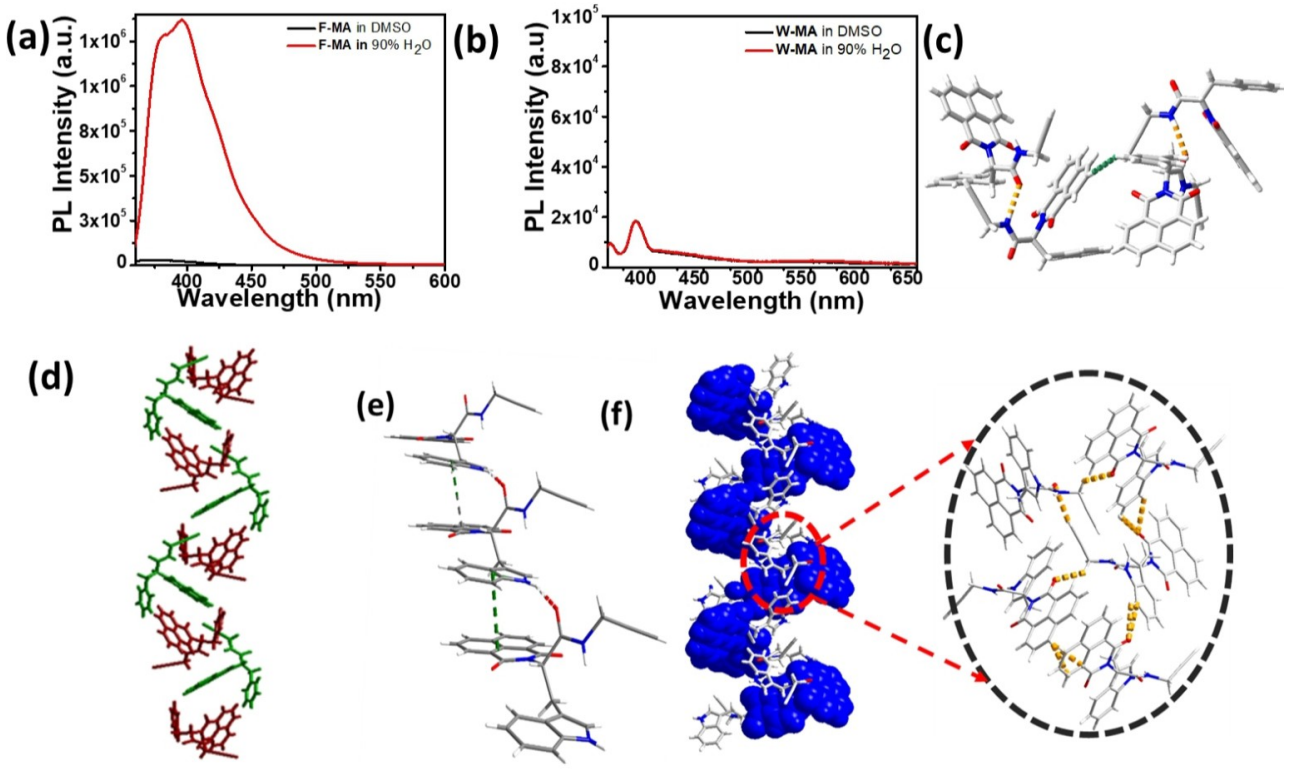

Figure 4. Fluorescence spectra of a) **F-MA** and b) **W-MA** in DMSO and 90% H_2O in DMSO (conc. 2×10^{-5} M), c) X-ray crystal structure of **F-MA** showing the interactions between two molecules. d) Helical structure of **F-MA**, e) X-ray crystal structure of **W-MA** showing hydrogen bonding between indole NH of Trp and amide carbonyl (red dots) and the intermolecular π–π interaction between NI and Trp (green dashed lines), f) The packing of **W-MA**, showing non-covalent interactions between naphthyl units are shown.

interactions play the dominant role in the aggregation process, and not hydrogen bonding.

The CD and microscopic analyses had revealed that in DMSO and in ACN, the dialkyne molecules are molecularly dispersed. Addition of water to DMSO solution, causes the on-start of hydrophobic interactions leading to aggregation. The sequestering of hydrophobic side chain of amino acid in presence of water is the cause for the observed fusion. The point chirality of amino acid induces an emergent chirality to the hydrophobically driven assembly. The role of water on the self-assembly process is depicted in Scheme 1. This hydrophobically driven assembly is the cause for inducing the fluorescence, as presented in the earlier section. Presence of water in the medium, causes the segregation of hydrophobic groups resulting in the aggregation leading to AIE.

The helical supramolecular polymers have several applications in chiral guest binding, asymmetric catalysis and in material science.[1a] The chiral supramolecular systems could act as dopants by binding with and directing the matrix molecules, thereby tuning their material properties.

The chiral AIE molecules as dopants to liquid crystalline material are desirable choices since they could induce chiral phases with high luminescence intensity in their aggregation state.[23] Therefore, such AIE luminogens (AIEgens) are excellent materials for the development of full-color photonics and dual-mode display devices.[24,25] The doping based

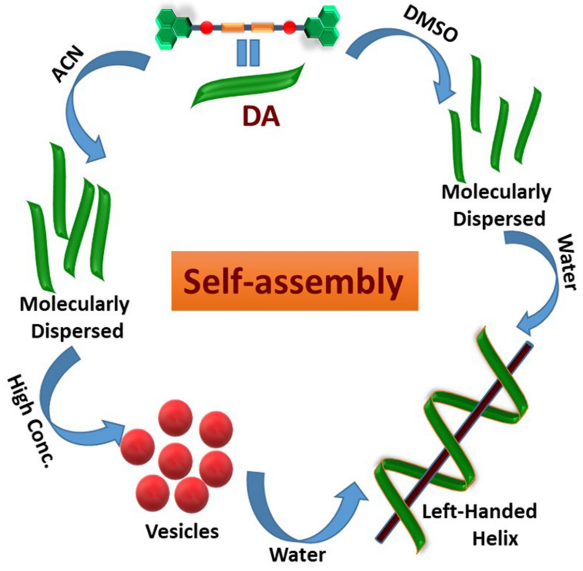

Scheme 1. Self-assembly pathways of diacetylene molecules in ACN and dimethylsulfoxide (DMSO) upon modulation of solvent and concentration conditions.

on the supramolecular approach is an efficient way to tune material properties, which pave the way for future materials. In order to investigate the utility of these self-assembling

dialkynes as a dopant, we analyzed various mixtures of dialkynes and LC. The induction of chirality and luminescent properties into the LC material can serve in the development of advanced optical materials.[23–27]

To test the dialkynes as chiral dopants, we used 4-cyano-4′-pentylbiphenyl (**5CB**) as a non-chiral LC host. We prepared various mixtures of **5CB** and **F-DA** dialkyne. The addition of 0.2 and 0.5 wt% of **F-DA** to the **5CB** showed almost no effect on the isotropic to nematic phase transition temperature (T_{NI}). At higher **F-DA** concentrations (0.75–5 wt%), the T_{NI} value reduced from 34.5 to 30.5 °C (Figure S49a). The textural investigation was performed for various mixtures of **5CB** and **F-DA** at room temperature after cooling from the isotropic to nematic state (Figure 5). The pure **5CB** exhibits the Schlieren texture with curved dark brushes.[28] The mixtures at concentrations from 0.2 to 1 wt% of **F-DA** exhibit fingerprint textures which are the characteristic feature of helical cholesteric phases. At 1 wt% and higher concentrations of **F-DA**, the texture of **5CB** changed from Schlieren to broken fans with fingerprints (Figure 5). The **F-DA** dopant induces the helicoidal cholesteric structures in the achiral nematic phases of the LCs (Figure 5j). The pitch of the induced cholesteric phases has been calculated by measuring the distance between the two neighboring extinction dark striations of cholesteric fingerprints.[24,28] Via the amount of doping agent, we could control the pitch of the helix. The helical twisting power (β)

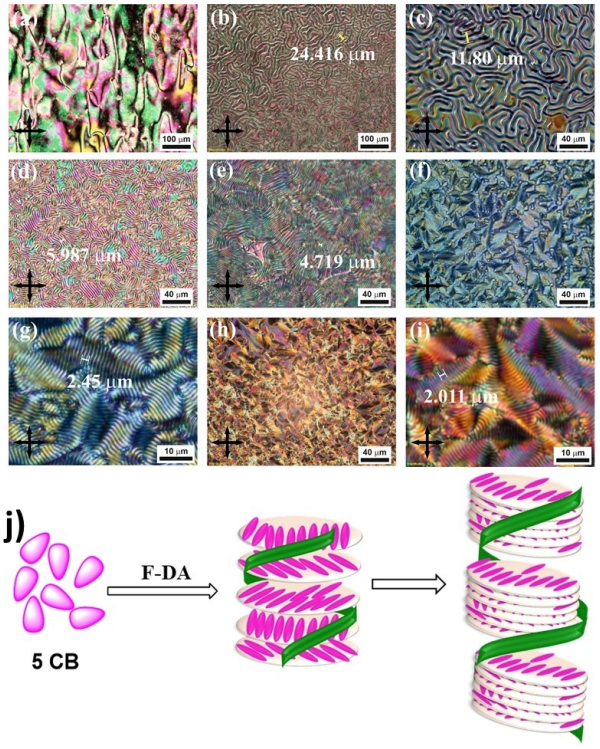

Figure 5. The POM micrographs of **5CB** doped with **F-DA** chiral agent on untreated glass slide a) 0 wt% b) 0.2 wt% c) 0.5 wt% d) 0.75 wt% e) 1 wt% f) 2 wt% g) Magnified-2 wt% h) 5 wt% i) Magnified-5 wt%, j) Representation of the chiral amplification to achiral LC by addition of **F-DA** compound.

remains invariant at lower concentrations of chiral dopants.[29] A high value of $\beta = 20.57\ \mu m^{-1}$ (Figure S49) is obtained for **F-DA**. These dialkynes may find applications in solar cell concentrators, bioprobes, chemosensor and imaging techniques.[23,30] The addition of non-chiral Aib-based dialkynes (**B-DA**) showed no effect on the textural features of **5CB**.

The handedness of the helix was ascertained by a miscibility test and by analyzing the sense of rotation of the double spiral formed under spherical wedge geometry.[31] For the miscibility test, the three commercially available chiral dopants 4-Cyano-4′- (2-methylbutyl)-biphenyl (**CB15**), S-(+)-2-Octyl 4-(4- hexyloxybenzoyloxy) benzoate (**S811**) and cholesteryl oleyl carbonate (**COC**) are used. The **S811** and **COC** are known to induce left-handed, while **CB15** show right-handed cholesteric phases. The mixture of 3 wt% **F-DA** with **5CB** and **CB15** doped **5CB** showed continuous contact (Figure S50a) in POM imaging indicating the induction of the right-handed helix in the cholesteric phase. On the other hand, **S811** and **COC** doped **5CB** showed a discontinuous boundary at the contact region (Figure S50b–c). The miscibility test confirms that **F-DA** induces a right-handed cholesteric phase. Apart from the miscibility test, the sense of rotation of the double spiral (Figure S51) further confirms the handedness. These self-assembling dialkynes are new class of chiral dopants with high potential for developing novel optical materials.

The higher β of **F-DA** than commercially available dopants such as **CB15**, **S811**, and **COC** indicates promising future for these designer dopants. Peptide-based compounds are likely to have better biocompatibility, unlike other synthetic dopants. These chiral molecules could also serve as dopants to other liquid crystals. The newly engineered peptides with the AIE characteristics allow us to fabricate luminescent liquid crystals with a high dichroic ratio. Attaching switchable moieties to these dopants, is another avenue for engineering stimuli responsive LCs. Apart from supramolecular chirality and AIE features, the cholesteric LC based systems may have potential applications in biosensing.[32]

In conclusion, we have presented the hydrophobically driven self-assembly of diacetylene pseudopeptide compounds that showed strong AIE behavior. Amino acids provide innumerable opportunities for designing hydrophobically driven self-assembled materials. Detailed spectroscopic and crystallographic studies revealed chiral supramolecular organization. Microscopic analyses of these diacetylene compounds revealed that increasing concentration leads to vesicular self-assembly in ACN, while addition of water changed the morphology to fibers with AIE. Replacing amide linkages with ester, retained the AIE, giving the evidence that hydrophobic interaction is the predominant contributor to aggregation. The AIE peptides serve as excellent dopants for modulating the properties of liquid crystals. These compounds, which themselves are not liquid crystalline, could be used as a director of LC organization in an unprecedented fashion. This opens up innumerable avenues for the design of supramolecular dopants. Overall, we designed and synthesized a novel set of

molecules that assemble to chiral aggregates driven by hydrophobic interactions and with chiral information controlled by the appended amino acids. These molecules are found to act as excellent dopant to LC with high helical twist. This work highlights that self-assembling dialkynes are new class of dopants that have high potential for developing new optoelectronic materials.

Acknowledgements

We acknowledge the funding (grant number EMR/2017/003192/OC) from the Science & Engineering Research Board (SERB), Government of India. GPM thanks the University Grants Commission (UGC) for the doctoral fellowship. We thank Prof. Paloth Venugopalan for help in X-ray structure analysis.

Conflict of Interest

The authors declare no conflict of interest.

Data Availability Statement

The data that support the findings of this study are available in the supplementary material of this article.

Keywords: Aggregation-Induced Emission · Liquid Crystal · Pseudopeptides · Self-Assembly · Supramolecular Helix

[1] a) E. Yashima, N. Ousaka, D. Taura, K. Shimomura, T. Ikai, K. Maeda, *Chem. Rev.* **2016**, *116*, 13752–13990; b) Q. Luo, C. Hou, Y. Bai, R. Wang, J. Liu, *Chem. Rev.* **2016**, *116*, 13571–13632; c) H. S. Martin, K. A. Podolsky, N. K. Devaraj, *ChemBioChem* **2021**, *22*, 3148–3157; d) S. V. Luis, I. Alfonso, *Acc. Chem. Res.* **2014**, *47*, 112–124.

[2] a) K. Petkau-Milroy, L. Brunsveld, *Org. Biomol. Chem.* **2013**, *11*, 219–232; b) Y. Sang, M. Liu, *Chem. Sci.* **2022**, *13*, 633–656.

[3] a) V. Haridas, *Acc. Chem. Res.* **2021**, *54*, 1934–1949; b) E. C. Das, S. Dhawan, J. Babu, P. Anil Kumar, T. V. Kumary, V. Haridas, M. Komath, *J. Periodontal Res.* **2019**, *54*, 468–480; c) V. Haridas, S. Sadanandan, P.-Y. Collart-Dutilleul, S. Gronthos, N. H. Voelcker, *Biomacromolecules* **2014**, *15*, 582–590; d) A. Bhattacharya, R. J. Brea, N. K. Devaraj, *Chem. Sci.* **2017**, *8*, 7912–7922.

[4] a) R. J. Brea, N. K. Devaraj, *Nat. Commun.* **2017**, *8*, 730; b) Y. Chen, Y. Bai, Z. Han, W. He, Z. Guo, *Chem. Soc. Rev.* **2015**, *44*, 4517–4546; c) T. L. Mako, J. M. Racicot, M. Levine, *Chem. Rev.* **2019**, *119*, 322–477.

[5] a) G. Feng, B. Liu, *Acc. Chem. Res.* **2018**, *51*, 1404–1414; b) S. Reineke, F. Lindner, G. Schwartz, N. Seidler, K. Walzer, B. Lüssem, K. Leo, *Nature* **2009**, *459*, 234–238.

[6] a) J. Mei, N. L. C. Leung, R. T. K. Kwok, J. W. Y. Lam, B. Z. Tang, *Chem. Rev.* **2015**, *115*, 11718–11940; b) X. Cai, B. Liu, *Angew. Chem. Int. Ed.* **2020**, *59*, 9868–9886; *Angew. Chem.* **2020**, *132*, 9952–9970.

[7] N. Na, X. Mu, Q. Liu, J. Wen, F. Wang, J. Ouyang, *Chem. Commun.* **2013**, *49*, 10076.

[8] A. Sánchez-Ruiz, A. Sousa-Hervés, J. Tolosa Barrilero, A. Navarro, J. C. Garcia-Martinez, *Polymer* **2021**, *13*, 213.

[9] E. G. McRae, M. Kasha, *J. Chem. Phys.* **1958**, *28*, 721–722.

[10] D. Wang, B. Z. Tang, *Acc. Chem. Res.* **2019**, *52*, 2559–2570.

[11] R. Domínguez, M. Moral, M. P. Fernández-Liencres, T. Peña-Ruiz, J. Tolosa, J. Canales-Vázquez, J. C. García-Martínez, A. Navarro, A. Garzón-Ruiz, *Chem. Eur. J.* **2020**, *26*, 3373–3384.

[12] a) M. M. J. Smulders, A. P. H. J. Schenning, E. W. Meijer, *J. Am. Chem. Soc.* **2008**, *130*, 606–611; b) R. A. Palmans, E. W. Meijer, *Angew. Chem. Int. Ed.* **2007**, *46*, 8948–8968; *Angew. Chem.* **2007**, *119*, 9106–9126; c) I. De Cat, Z. Guo, S. J. George, E. W. Meijer, A. P. H. J. Schenning, S. De Feyter, *J. Am. Chem. Soc.* **2012**, *134*, 3171–3177.

[13] a) S. Huang, H. Yu, Q. Li, *Adv. Sci.* **2021**, *8*, 2002132; b) R. Garifullin, M. O. Guler, *Chem. Commun.* **2015**, *51*, 12470–12473; c) M. P. Hendricks, K. Sato, L. C. Palmer, S. I. Stupp, *Acc. Chem. Res.* **2017**, *50*, 2440–2448.

[14] a) Y. Zhao, L. J. Leman, D. J. Search, R. A. Garcia, D. A. Gordon, B. E. Maryanoff, M. R. Ghadiri, *ACS Cent. Sci.* **2017**, *3*, 639–646; b) J. Montenegro, M. R. Ghadiri, J. R. Granja, *Acc. Chem. Res.* **2013**, *46*, 2955–2965; c) G. Lu, Y. Chen, Y. Zhang, M. Bao, Y. Bian, X. Li, J. Jiang, *J. Am. Chem. Soc.* **2008**, *130*, 11623–11630; d) N. Mizoshita, S. Inagaki, *Angew. Chem. Int. Ed.* **2015**, *54*, 11999–12003; *Angew. Chem.* **2015**, *127*, 12167–12171.

[15] a) S. van Dun, C. Ottmann, L.-G. Milroy, L. Brunsveld, *J. Am. Chem. Soc.* **2017**, *139*, 13960–13968; b) A. H. A. M. van Onzen, L. Albertazzi, A. P. H. J. Schenning, L.-G. Milroy, L. Brunsveld, *Chem. Commun.* **2017**, *53*, 1626–1629; c) D. A. Uhlenheuer, K. Petkau, L. Brunsveld, *Chem. Soc. Rev.* **2010**, *39*, 2817.

[16] a) J. K. Kretsinger, J. P. Schneider, *J. Am. Chem. Soc.* **2003**, *125*, 7907–7913; b) K. McGuinness, I. J. Khan, V. Nanda, *ACS Nano* **2014**, *8*, 12514–12523.

[17] a) S. Wang, Y. Tao, J. Wang, Y. Tao, X. Wang, *Chem. Sci.* **2019**, *10*, 1531–1538; b) T. Wang, C. Ménard-Moyon, A. Bianco, *Chem. Soc. Rev.* **2022**, *51*, 3535–3560.

[18] a) S. Dhawan, A. Moudgil, H. Singh, S. Gahlawat, J. Babu, P. P. Ingole, S. Das, V. Haridas, *Mol. Syst. Des. Eng.* **2020**, *5*, 847–855; b) V. Haridas, Y. K. Sharma, R. Creasey, S. Sahu, C. T. Gibson, N. H. Voelcker, *New J. Chem.* **2011**, *35*, 303–309.

[19] D. Takajo, K. Sudoh, *Langmuir* **2019**, *35*, 2123–2128.

[20] a) F. Würthner, T. E. Kaiser, C. R. Saha-Möller, *Angew. Chem. Int. Ed.* **2011**, *50*, 3376–3410; *Angew. Chem.* **2011**, *123*, 3436–3473; b) C. Felip-León, F. Galindo, J. F. Miravet, *Nanoscale* **2018**, *10*, 17060–17069.

[21] B. D. McCarthy, E. R. Hontz, S. R. Yost, T. Van Voorhis, M. Dincă, *J. Phys. Chem. Lett.* **2013**, *4*, 453–458.

[22] a) K. Sugiyasu, N. Fujita, S. Shinkai, *Angew. Chem. Int. Ed.* **2004**, *43*, 1229–1233; *Angew. Chem.* **2004**, *116*, 1249–1253; b) Q. N. Pham, N. Brosse, C. Frochot, D. Dumas, A. Hocquet, B. Jamart-Grégoire, *New J. Chem.* **2008**, *32*, 1131.

[23] J. Voskuhl, M. Giese, *Aggregate* **2022**, *3*, e124.

[24] Q. Xia, L. Meng, T. He, G. Huang, B. S. Li, B. Z. Tang, *ACS Nano* **2021**, *15*, 4956–4966.

[25] J. Li, H. K. Bisoyi, J. Tian, J. Guo, Q. Li, *Adv. Mater.* **2019**, *31*, 1807751.

[26] a) L. Wang, A. M. Urbas, Q. Li, *Adv. Mater.* **2020**, *32*, 1801335; b) J. Guo, X.-L. Li, H. Nie, W. Luo, S. Gan, S. Hu, R. Hu, A. Qin, Z. Zhao, S.-J. Su, B. Z. Tang, *Adv. Funct. Mater.* **2017**, *27*, 1606458.

[27] D. Zhao, H. He, X. Gu, L. Guo, K. S. Wong, J. W. Y. Lam, B. Z. Tang, *Adv. Opt. Mater.* **2016**, *4*, 534–539.

[28] I. Dierking, in *Textures of Liquid Crystals*, Wiley-VCH, Weinheim, **2003**.

[29] S. Pieraccini, A. Ferrarini, G. P. Spada, *Chirality* **2008**, *20*, 749–759.

[30] X. Zhang, H. Liu, G. Zhuang, S. Yang, P. Du, *Nat. Commun.* **2022**, *13*, 3543.
[31] a) A. Nemati, S. Shadpour, L. Querciagrossa, L. Li, T. Mori, M. Gao, C. Zannoni, T. Hegmann, *Nat. Commun.* **2018**, *9*, 3908; b) G. Heppke, F. Oestreicher, *Mol. Cryst. Liq. Cryst.* **1978**, *41*, 245–249.
[32] R. J. Carlton, J. T. Hunter, D. S. Miller, R. Abbasi, P. C. Mushenheim, L. N. Tan, N. L. Abbott, *Liq. Cryst. Rev.* **2013**, *1*, 29–51.

Manuscript received: July 5, 2022
Accepted manuscript online: August 25, 2022
Version of record online: September 12, 2022